Supplemental Information

Immature integration and segregation of emotion-related brain circuitry in young children

Shaozheng Qin [a*], *Christina B. Young* [a], *Kaustubh Supekar* [a], *Lucina Q. Uddin* [a], *Vinod Menon* [a,b,c,d*]

[a] Department of Psychiatry & Behavioral Sciences,

[b] Neurology and Neurological Sciences,

[c] Program in Neuroscience,

[d] Stanford Institute for Neuro-Innovation and Translational Neurosciences,

Stanford University School of Medicine, Stanford, CA 94304

* Corresponding author(s)

Table of content

Text S1

Materials and Methods

Participants. Two cohorts of children and adults (N = 87 in total) participated in this study after giving written, informed consent. The first cohort consisted of 24 typically developing children, and 24 young healthy adults who were selected from narrow age ranges (7 to 9 years for children, 19 to 22 years for adults) to minimize age-related variability within each group. A second independent cohort of 23 children and 16 healthy adults was used for replication analyses. The study protocol was approved by the Stanford University Institutional Review Board. Participants reported no history of neurological or psychiatric diseases, and no current use of any medication or recreational drugs. All participants had IQ above 90 and below 130. IQ was measured using the Wechsler Abbreviated Scales of Intelligence (WASI), and full scale IQ scores were normalized in terms of corresponding age for children and adults. For children, written informed consent was obtained from their legal guardian. Demographic data including age and gender along with head motion parameters for fMRI data are shown in *Table S1 below*. The children and adult groups did not differ in gender distribution or IQ, as well as head motion during scanning.

Data acquisition. For the resting-state fMRI scan, participants were instructed to keep their eyes closed and remain still for a duration of the 8-min scan. Whole brain functional images were acquired on a 3T GE Signa scanner (General Electric, Milwaukee, WI) using a custom-built head coil with a T2*-sensitive gradient echo spiral in-out pulse sequence based on blood oxygenation level-dependent (BOLD) contrast (1). Twenty-nine axial slices (4.0 mm thickness, 0.5 mm skip) parallel to the AC–PC line and covering the whole brain were imaged with the following parameters: volume repetition time (TR) 2.0 sec, echo time (TE) 25 ms, 80° flip angle, matrix size 64 × 64, field of view 200 x 200 mm, and an in-plane spatial resolution of 3.125 mm. To reduce blurring and signal loss arising from field inhomogeneities, an automated high-order shimming method based on spiral acquisitions was used before acquiring functional images. A linear shim correction was applied separately for each slice during reconstruction using a magnetic field map acquired automatically by the pulse sequence at the beginning of the scan (2). A total of two hundred forty volumes were acquired during the resting-state scan.

Data preprocessing. Image preprocessing was performed using SPM8 (http://wwwfil.ion.ucl.ac.uk/spm). The first eight volumes were discarded for stabilization of the

MR signal. Remaining functional images were realigned to correct for rigid-body motion. Subsequently, images were slice-timing corrected, normalized into a standard stereotactic space, and resampled into 2 mm isotropic voxels. Finally, images were spatially smoothed by convolving an isotropic 3D-Gaussian kernel (6-mm full width at half maximum).

Regions of interest definition. Two regions of interest (ROIs) encompassing the BLA and CMA were created using cytoarchitectonically-defined probabilistic maps of the amygdala (illustrated *below*). Maximum probability maps were used to create non-overlapping amygdala subregions using the Anatomy Toolbox. Voxels were included in the maximum probability maps only if the probability of their assignment to the BLA or CMA was higher than any other nearby structures with greater than 40% likelihood. Each voxel was exclusively assigned to only one region. Overlapping voxels were assigned to the region that had the greatest probability, resulting in four non-overlapping ROIs representing CMA and BLA subregions in left and right hemispheres. There were 317 and 334 voxels in the left and right BLA, 53 and 69 voxels in the left and right CMA, respectively. To mitigate potential confounds related to differences in the size of the amygdala, we also analyzed the data using the first eigenvalue, rather than mean, of the ROI time series. The results were nearly identical to our original analyses (*Fig. S8*).

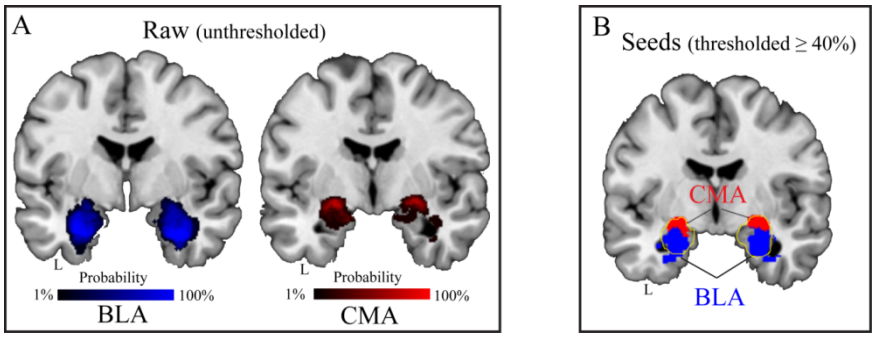

Observer-independent cytoarchitectonically-defined probabilistic maps of the basolateral (BLA) and central medial (CMA) amygdala subregions. (**A**) A representative coronal view of the cytoarchitectonically-defined probabilistic maps of the BLA and CMA (unthresholded). (**B**) A representative coronal view of the cytoarchitectonically-defined BLA and CMA thresholded with $p \geq 0.40$. Cytoarchitecture of the amygdala subregions was derived from a sample of ten human postmortem brains (3). The centromedial complex is coded in red, and the basolateral complex is coded in blue.

Cytoarchitectonic maps of the BLA and CMA have previously been proven to show high reliability and accuracy for guiding anatomical segmentation of amygdala subregions in children as young as 6 to 7 years old (4), as summarized in *Text S2 below*, indicating the feasibility and

validity of applying them to 7-9 year old children in our study. Using the same approach, two additional subregions (*Fig. S1&2 below*) in ventral visual cortex were defined that served as control regions in resting-state functional connectivity analyses.

Functional connectivity analysis. Regional time series within each seed ROI (averaging across all voxels) were extracted from data that was filtered with a bandpass temporal filter (0.008 to 0.10 Hz). Subsequently, each time series was submitted into an individual level fixed-effects analysis under the framework of the general linear model in SPM8. A global signal regressor and six motion parameters for each participant were included as covariates of no interest in the model to account for physiological noise and movement-related artifacts. For each participant, four separate functional connectivity analyses were performed for both BLA and CMA in left and right hemispheres.

The contrast parameter images for each of the four seed regions from the individual level analyses were submitted to a second-level group analysis that treated participants as a random variable in a two-by-two-by-two full factorial analyses of variance (ANOVA), with amygdala Subregion (BLA vs. CMA) and Hemisphere (left vs. right) as within-subject factors, and Group (adults vs. children) as a between-subjects factor. Since there was no significant interaction effect related to the factor of Hemisphere, contrasts of interest on group-level analyses were conducted collapsing across both hemispheres. Significant clusters were estimated using a height threshold of $p < 0.001$ uncorrected, and family-wise-error corrections for multiple spatial comparisons using an extent threshold of $p < 0.05$. The extent threshold was based on non-stationary suprathreshold cluster-size distributions computed using Monte Carlo simulations (5).

To characterize differential patterns of BLA and CMA target networks in children and adults, complementary ROI analyses were conducted using MarsBar (6). Masks for target networks of interest were anatomically defined by using the WFU PickAtlas toolbox (7). We selected these networks because they comprise canonical brain regions (see *Fig. S6 below*) involved in various affective and cognitive functions (8-10): (1) several subcortical areas including striatum, thalamus and midbrain known to play a critical role in reward and motivation; (2) crus and vermis/declive regions of the cerebellum are known to play an important role in regulating fear-related defensive and reflective responses; (3) unimodal and polymodal association areas, including visual cortex (VC), parahippocampal gyrus (PHG), inferior temporal cortex (ITC), middle (MTG) and superior temporal gyrus (STG), premotor cortex (PMC) and sensorimotor

cortex (SM), are crucial for perception of affective information; (4) limbic and paralimbic structures, including hippocampus (Hipp), insula (Ins), and middle (mCC) and posterior (PCC) portions of cingulate cortex, contribute to regulation of arousal, positive and negative affect and motivation; and (5) prefrontal cortex, including anterior cingulate cortex (ACC), middle (MFG) and inferior gyrus (IFG), and medial prefrontal cortex (MPFC), are important for emotional appraisal and regulation. Mean parameter estimates (or β weights), representing the strength of functional connectivity of each seed with corresponding target masks, were extracted from BLA- and CMA-seeded functional connectivity analyses. These data were then submitted to further statistical testing in SPSS 18.0 (SPSS Inc, Chicago, Illinois).

Spatial correlations, reflecting similarity between BLA and CMA connectivity, were computed between each participant's unthresholded BLA- and CMA-seeded functional connectivity maps within a mask representing overall amygdala connectivity network collapsing across adults and children. Each participant's unthresholded BLA- and CMA-seeded connectivity maps was first reshaped into one dimensional vectors, and Pearson correlation coefficients between vectors were computed. This yields a numerical measure of the spatial similarity between connectivity maps, analogous to similarity metrics that have been used in resting state as well as task-related fMRI data (11-14). Thus, higher spatial correlation indicates higher similarity between the two target networks. We used this approach because it allows us to quantify the overall similarity between the BLA and CMA target networks, and, furthermore, to examine quantitative differences in the similarity of the target networks between children and adults. In addition, temporal correlations between BLA and CMA seeds were calculated on the basis of their bandpass-filtered time series in ipsilateral and contralateral hemispheres in order to specifically investigate developmental differences in interregional coupling of BLA and CMA. Corresponding correlation coefficients were then Fisher's *Z*-transformed for further statistical testing in SPSS.

Text S2

Validity of using cytoarchitectonic probabilistic maps in children. No cytoarchitectonic probabilistic maps of the BLA and CMA in children are currently available, findings from one recent postmortem case study suggests that the relative subregional positions and proportions of anatomical boundaries are likely similar in children and adults (4). Specifically, Kim and colleagues found that amygdala subregional boundaries from the postmortem brain of a 10-year-old boy were not different from cytoarchitectonic boundaries of the BLA and CMA based on a sample of ten adult postmortem brains (*see* (4) for *original figures*). Crucially, these cytoarchitectonic probabilistic maps had been shown to have high reliability and accuracy for guiding anatomical segmentation of amygdala subregions in children as young as 6- to 7-year-old (4), indicating the feasibility and validity of applying these adult maps to children.

We undertook several steps to minimize potential sources of confounds in our analysis as well as interpretation of findings. We used a nonlinear transformation procedure to accurately map each child and adult brain to the same target space as the BLA and CMA cytoarchitectonic probability maps used here. By normalizing individual brains into a stereotaxic standardized space, this general approach has been validated across many neurodevelopmental studies (15-19), which can mitigates individual variability in anatomy and brain size and thereby allowing us to conduct appropriate developmental studies.

Finally, our use of the control regions provides further validation for the specificity of our findings. Control analyses performed by using ventral visual cortical subregions (i.e., V1 and V2; *Figure S1 and S2*) did not find any significant interaction between group (children vs. adults) and visual subregions (V1 vs. V2). In other words, there are no significant developmental changes in dissociation of these two subregional networks, although we found a general dissociation of connectivity patterns between these visual subregions for both adults and children. The contrary patterns of results observed in visual cortical (V1 vs. V2) and amygdala (BLA vs. CMA) subregions suggest the validity of applying the BLA and CMA probabilistic maps to children, as one would expect a generally consistent, i.e., null group-by-subregion interaction (see *Figure S2*) if this method failed. Taken together, pending the publication of pediatric cytoarchitectonic maps of the amygdala and our control analyses, our methods are valid and reliable.

Tables S1-S6

Table S1. Participant demographics and motion parameters during fMRI scanning

		Adults	Children	2nd Adults	2nd Children
N		24	24	16	23
Age (range)		20.56 (19 - 22)	8.11 (7 - 9)	24.06 (19 - 30)	8.41 (7 - 9)
Gender		12 M / 12 F	12 M / 12 F	8 M / 8 F	11 M / 12 F
IQ (mean ± SD)		112.59 ± 10.38	110.33 ± 10.17	-	111.45 ± 10.32
Motion parameters (mean ± SD)	X (mm)	0.184 ± 0.098	0.225 ± 0.107	0.698 ± 0.149	0.285 ± 0.110
	Y (mm)	0.314 ± 0.139	0.334 ± 0.198	0.404 ± 0.150	0.354 ± 0.177
	Z (mm)	0.716 ± 0.482	0.622 ± 0.328	0.994 ± 0.225	0.722 ± 0.388
	Pitch (°)	0.014 ± 0.009	0.013 ± 0.005	0.019 ± 0.004	0.009 ± 0.004
	Roll (°)	0.006 ± 0.003	0.008 ± 0.004	0.012 ± 0.002	0.007 ± 0.004
	Yaw (°)	0.005 ± 0.003	0.006 ± 0.003	0.013 ± 0.003	0.006 ± 0.005

Notes: F, female; M, male; N, number of participants; SD - standard deviation; 2nd Adults and 2nd Children, the second cohorts of adult and children participants respectively. Motion parameters - six motion parameters (translation: x, y and z in mm; rotation: pitch, roll and yaw in degrees) were obtained from head movement correction for each participant.

Table S2. Brain regions that show weaker functional connectivity with amygdala in children compared to adults

Brain regions		R/L	BA	T values	MNI (x, y, z)
Main effect of group: Adults versus Children					
Limbic and paralimbic structures	Cingulate gyrus	L	24	5.13 [a]	0 -2 46
	Insula	L	13	5.09 [a]	-32 -10 -8
		R		5.39 [a]	40 -4 6
	PRC	R	20	5.95 [a]	30 -8 -34
Subcortical structures	Caudate	L	-	4.93 [a]	-6 0 10
		R		5.62 [a]	10 2 10
	Putamen	L	-	4.61 [b]	-28 10 -6
		R		4.72 [b]	32 12 2
	Midbrain & Brainstem	-	-	5.36 [a]	0 -32 -16
		R		5.13 [a]	6 -38 -22
	Cerebellum	L	-	3.80 [b]	-28 -64 -20
		R		4.73 [b]	8 -44 -10
Polymodal association areas	SPL	R	7	5.55 [a]	8 -66 54
	SM &PMC	L	4,3	4.41 [b]	-36 -32 64
		R		4.25 [b]	22 -26 64
	STG & MTG	L	22	5.49 [a]	-58 2 -6
		R		4.68 [b]	60 -12 8
	ITC	L	39	5.67 [a]	-40 -76 12
		R		4.68 [b]	48 -76 16
Prefrontal cortices	MFG	L	8	5.43 [a]	-26 32 46
		R		5.28 [a]	30 32 44
	VMPFC	L	10	4.04 [b]	6 50 4
		R		3.88 [b]	0 52 4

Notes: Only clusters significant at $p < 0.05$, corrected at the cluster level, are reported with local maxima in Montreal Neurological Institute (MNI) standard space. Data from the second cohort of children are not shown. Abbreviations: BA, Brodmann's area; MFG, middle prefrontal gyrus; MTG, middle temporal gyrus; PMC, premotor cortex; PRC, perirhinal cortex; SPL, superior parietal lobe; SM, sensorimotor areas; VMPFC, ventromedial prefrontal cortex; L, left hemisphere; R, right hemisphere; [a], $p < 0.05$ FWE whole brain corrected; [b], cluster $p < 0.05$ corrected; -, no proper data.

Table S3. Brain regions that show significant interaction effects between and amygdala subregions.

Brain regions		R/L	BA	Adults	
				T values	MNI (x, y, z)
Interaction effect: Group (Adults vs. Children) x Subregion (CMA vs. BLA)					
Subcortical structures	Thalamus	L	-	4.30 [b]	-12 -12 12
		R		5.76 [a]	2 -14 8
	Hippocampus	L	-	4.01 [b]	-20 -42 10
	Caudate	L	-	3.52 [b]	-18 -22 20
		R		3.74 [b]	20 -22 20
	Cerebellum	L	-	4.81 [b]	-30 -72 -28
		R		3.39 [b]	16 -78 -24
Interaction effect: Group (Adults vs. Children) x Subregion (BLA vs. CMA)					
Polymodal association areas	STG & MTG	L	20	4.20 [b]	-52 -36 -6
		R	21	4.68 [b]	64 -28 -4
	SM	L	4,3	4.03 [b]	-48 -26 42
		R		3.96 [b]	46 -16 36
	VC	L	19	4.66 [b]	-20 -86 20
		R		4.34 [b]	16 -88 26
		L	17,18	4.57 [b]	-12 -80 -2
		R		3.74 [b]	16 -82 -2
	ITC	R	37	3.81 [b]	46 -66 -2

Notes: SM, sensorimotor cortex; VC, visual cortex. Other notes and abbreviations are same as that in Table 2.

Table S4. Brain regions that show significant differences in functional connectivity between CMA versus BLA, computed separately in adults and children

Brain regions		R/L	BA	Adults		Children	
				T values	MNI (x, y, z)	*T* values	MNI (x, y, z)
Contrast: CMA versus BLA							
Limbic	Amygdala	L	-	5.70 [a]	-24 -6 -8	5.69 [a]	-24 -6 -6
		R		6.80 [a]	28 -8 -8	6.63 [a]	28 -6 -8
	Hippocampus	L	-	5.08 [a]	-18 36 10	-	-
		R		4.37 [b]	28 -10 -12	-	-
	Cingulate gyrus	R	24	3.85 [b]	2 16 38	-	-
Subcortical	Thalamus	L	-	6.22 [a]	-14 -22 18	-	-
		R		7.37 [a]	2 -14 8	-	-
	Putamen	L	-	6.12 [a]	30 -8 -8	-	-
		R		5.35 [a]	-26 -8 -8	-	-
	Pallidum	L	-	6.25 [a]	28 -8 -6	-	-
		R		5.54 [a]	-22 -8 -6	-	-
	Caudate	L	-	5.55 [a]	-16 -18 20	-	-
		R		5.72 [a]	20 -22 20	-	-
	Midbrain	L	-	5.25 [a]	2 -34 0	-	-
		R		4.31 [b]	-6 -8 -2	-	-
	Cerebellum	L	-	4.78 [b]	-10 -84 -24	-	-
		R		4.66 [b]	22 -78 -24	-	-
Contrast: BLA versus CMA							
(Para)Limbic structures	Amygdala	L	-	6.71 [a]	-22 -6 -24	7.03 [a]	-26 -4 -22
		R		6.93 [a]	28 -6 -28	7.32 [a]	26 -4 -26
	PRC	L	20	4.66 [a]	-30 -24 -22	5.09 [a]	-36 -12 -28
		R		4.93 [a]	30 -20 -24	5.50 [a]	42 -16 -32
	TP	L	21	5.04 [a]	-48 0 -28	4.16 [b]	-36 12 -38
		R		4.57 [b]	56 2 -24	4.85 [b]	40 18 -36
Polymodal association areas	STG & MTG	L	22	4.21 [b]	-60 -30 4	-	-
		R		4.67 [b]	64 -34 6	-	-
	MC	L	3	4.47 [b]	-4 -22 60	-	-
		R		4.10 [b]	14 -34 72	-	-
	IPL	L	40	5.46 [a]	-50 -26 44	-	-
		R		4.63 [b]	50 -26 48	-	-
	PAC	L	41	4.33 [b]	-40 -38 14	-	-
		R		4.49 [b]	48 -30 10	-	-
	VC	L	19	5.75 [a]	-20 -84 32	-	-
		R		5.31 [a]	18 -84 34	-	-
		L	17,18	5.15 [a]	-12 -80 -2	-	-
		R		4.40 [b]	14 80 -2	-	-

Notes: PAC, primary auditory cortex; MC, primary motor cortex; IPL, inferior parietal cortex; TP, temporal pole. Other notes and abbreviations are the same as that in Table S2 and Table S3;

Table S5. Brain regions that show significant functional connectivity with the BLA in adults and children

Brain regions		R/L	BA	Adults		Children	
				T values	MNI (x, y, z)	*T* values	MNI (x, y, z)
(Para)Limbic	Amygdala	L	-	14.12 [a]	-24 -4 -18	18.66 [a]	-26 -4 -18
		R		13.35 [a]	28 -4 -24	17.41 [a]	26 -4 -22
	Hippocampus	L	-	6.62 [a]	-24 -34 -6	6.72 [a]	-22 -34 -6
		R		6.40 [a]	22 -32 -6	9.26 [a]	28 -22 -16
	Insula	L	13,14	8.85 [a]	-40 -4 -10	7.57 [a]	36 -16 18
		R		8.07 [a]	-36 -16 10	7.28 [a]	-32 -20 14
	Cingulate gyrus	L	24	7.14 [a]	-2 -14 50	4.91 [a]	-8 -14 50
		R		6.31 [a]	6 -18 54	5.33 [a]	8 -14 54
	PRC	L	20	8.86 [a]	-30 -8 -32	10.65 [a]	-36 -12 -28
		R		11.48	30 -6 -34	9.30 [a]	44 -16 -30
	TP	L	20,21	7.26 [a]	-48 2 -28	10.06 [a]	-36 14 -40
		R		8.62 [a]	36 6 -30	9.32 [a]	40 18 -38
	PHC	L	36	8.91 [a]	-34 -42 -22	9.47 [a]	-34 -38 -24
		R		9.84 [a]	32 -34 -22	8.19 [a]	32 -34 -22
Subcortical structures	Thalamus	L	-	10.32 [a]	-6 -20 8	7.44 [a]	10 -30 2
		R		10.52 [a]	8 -20 8	7.36 [a]	-8 -30 0
	Putamen Pallidum	L	-	7.69 [a]	-32 -12 -8	10.97 [a]	-24 -4 -8
		R		7.95 [a]	36 -12 -6	9.74 [a]	28 -2 -8
	Caudate	L	-	6.15 [a]	-10 0 12	7.37 [a]	6 8 -6
		R		6.07 [a]	-6 0 12	6.48 [a]	-4 10 -6
	Midbrain	L	-	7.35 [a]	-8 -30 -4	10.88 [a]	-16 -12 -10
		R		7.23 [a]	10 -28 -4	9.21 [a]	18 -12 -12
	Brainstem	L	-	7.41 [a]	-4 -24 -28	6.15 [a]	-4 -24 -22
		R		5.99 [a]	10 -30 -36	4.53 [b]	10 -28 -38
	Cerebellum	L	-	5.96 [a]	-14 -46 -20	5.14 [a]	-16 -60 -32
		R		5.81 [a]	16 -48 -30	6.03 [a]	18 -56 -28
Polymodal association areas	SM	L	3, 4	7.51 [a]	-36 -34 64	4.04 [b]	-40 -18 50
		R		5.67 [a]	30 -26 66	5.51 [a]	62 -10 46
	STG & MTG	L	22	6.67 [a]	-56 -8 -14	6.89 [a]	-58 -10 -14
		R		7.51 [a]	58 0 -14	6.14 [a]	56 -10 -16
	PAC	L	41	6.01 [a]	-50 -36 10	4.65 [b]	-46 -24 6
		R		6.87 [a]	48 -30 10	4.76 [b]	52 -16 -2
	ITC & FG	L	37	6.94 [a]	-46 -76 -2	6.53 [a]	-46 -48 -20
		R		6.99 [a]	48 -66 0	6.61 [a]	50 -48 -20
	VC	L	19	6.31 [a]	-22 -70 -4	6.64 [a]	-16 -56 10
		R		7.26 [a]	20 -62 -10	5.22 [a]	14 -58 14
		L	17,18	5.94 [a]	-18 -82 36	4.63 [a]	-10 -96 -6
		R		6.35 [a]	20 -80 36	4.17 [b]	4 -92 -8
Prefrontal cortices	MPFC	L	10	5.12 [a]	-4 56 -12	6.32 [a]	-10 46 -14
		R		5.16 [a]	6 54 -10	7.14 [a]	6 50 -14
	IFG	L	11	6.10 [a]	-36 30 -18	6.81 [a]	-26 32 -14
		R		4.63 [b]	36 30 -18	6.63 [a]	36 30 -18

Notes: IFG, inferior frontal gyrus; PHC, parahippocampal cortex. Other notes and abbreviations are same as that in Tables S2, S3 and S4.

Table S6. Brain regions that show significant function connectivity with the CMA in adults and children

Brain regions		R/L	BA	Adults		Children	
				T values	MNI (x, y, z)	*T* values	MNI (x, y, z)
(Para)Limbic structures	Amygdala	L	-	15.29 [a]	-26, -4, -10	20.58 [a]	-22 – 6 -8
		R		17.88 [a]	28, -8, -10	21.74 [a]	26 -4 -10
	Insula	L	13, 14	9.05 [a]	-36, -8, -6	8.39 [a]	-32 -18 4
		R		7.49 [a]	40, -2, -10	9.02 [a]	38 8 -12
	Hippocampus	L	-	6.62 [a]	-26 -18 -14	8.21 [a]	-26 -18 -10
		R		8.41 [a]	30 -18 -12	9.02 [a]	26 -18 -14
	PHC	L	36	7.23 [a]	-28 -36 -6	6.27 [a]	-24 -38 -10
		R		5.38 [a]	36 -32 -8	11.76 [a]	30 -46 -16
	Cingulate gyrus	L	24	7.42 [a]	-2 0 44	5.73 [a]	-6 6 42
		R		6.71 [a]	12 10 46	5.33 [a]	10 8 40
Subcortical structures	Thalamus	L	-	10.32 [a]	-6 -20 8	10.42 [a]	-18 -10 -2
		R		10.52 [a]	8 -20 8	9.60 [a]	20 -10 -2
	Putamen	L	-	14.74 [a]	-26 -6 -8	20.21 [a]	-24 -4 -8
		R		16.59 [a]	28 -8 -6	19.56 [a]	28 -2 -8
	Pallidum	L	-	13.94 [a]	-26 -10 -6	19.75 [a]	-22 -6 -6
		R		9.08 [a]	12 4 -2	20.84 [a]	26 -6 -6
	Caudate	L	-	9.86 [a]	-14 -8 16	8.31 [a]	8 10 -4
		R		9.74 [a]	14 -2 14	7.70 [a]	-10 -2 18
	Midbrain	L	-	8.29 [a]	-6 -28 -10	5.33 [a]	-2 -24 -14
		R		9.50 [a]	8 -26 -10	7.00 [a]	8 -18 -10
	Brainstem	L	-	5.96 [a]	-8 -38 -30	-	-
		R	-	5.35 [a]	6 -36 -28	-	-
	Cerebellum	L	-	7.28 [a]	-22 -64 -22	5.21 [a]	-24 -58 -32
		R		6.65 [a]	10 -64 -16	5.83 [a]	28 -46 -32
Polymodal association areas	PMC & SM	L	3,4	4.58 [b]	-12 -12 76	5.42 [a]	-46 -12 46
		R		4.10 [b]	48 -6 36	8.54 [a]	44 -12 36
	STG & MTG	L	22, 38	7.03 [a]	-58 2 -6	7.42 [a]	-58 -10 -12
		R		6.45 [a]	52 12 -12	7.27 [a]	58 -12 -16
	ITC&FG	L	37	4.69 [b]	-52 -60 -12	4.55 [b]	-40 -50 -14
		R		3.56 [b]	32 -56 -10	5.30 [a]	34 -58 -16
Prefrontal cortices	MPFC	L	10	4.42 [b]	-6 48 0	5.04 [a]	-8 50 -8
		-		4.27 [b]	0 50 0	6.54 [a]	8 50 -10
	IFG	L	11	4.85 [b]	-32 34 -10	5.85 [a]	-30 22 -12
		R		4.40 [b]	34 32 -6	7.00 [a]	36 28 -16

Notes: All notes and abbreviations are same as that in Table S2, S3 and S5.

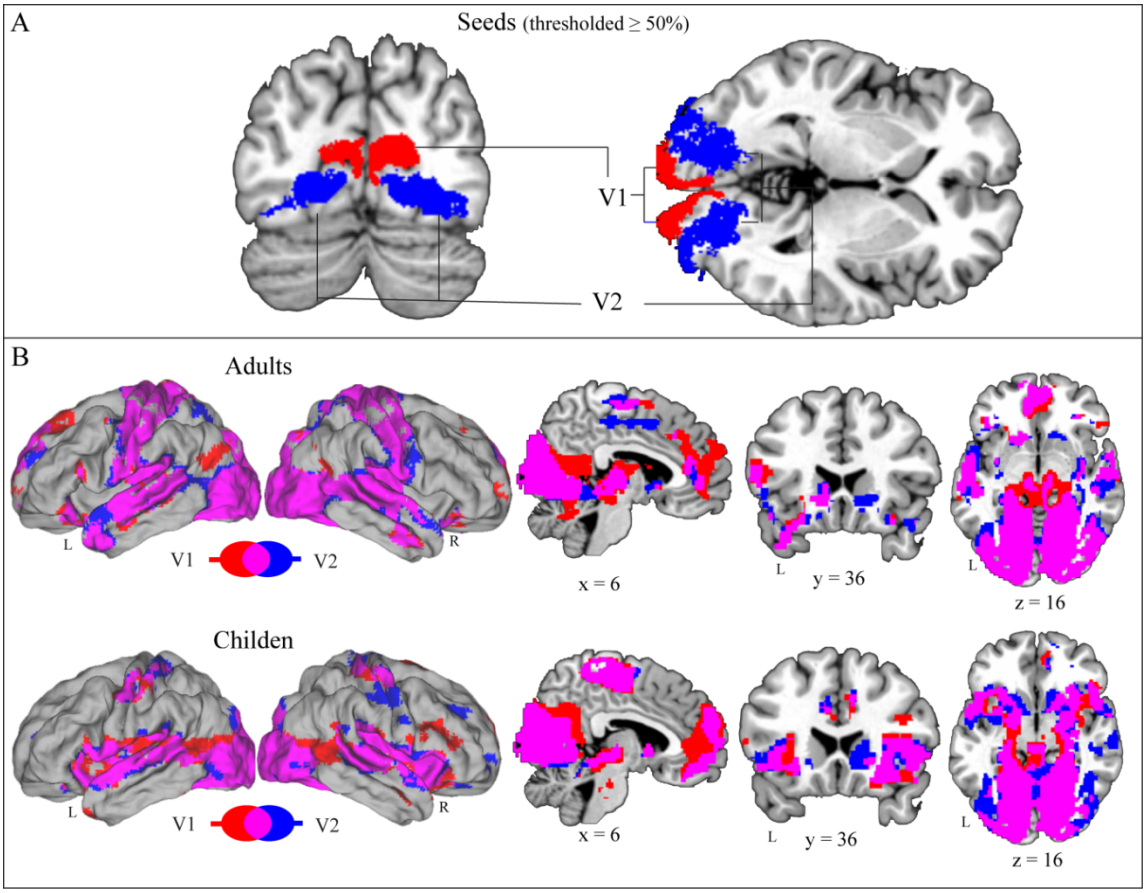

Fig S1. Observer-independent cytoarchitectonically-defined probabilistic maps of visual areas V1 and ventral part of V2 (20), and their functional connectivity in children and adults. (**A**) Representative coronal and axial views of V1 and ventral V2 (V2v) areas thresholded with p ≥ 0.50; (**B**) Brain regions that showed positive correlation with the V1 (shown in red) or the V2v (shown in blue; overlapping areas shown in pink) in 19-22 year-old adults and 7-9 year-old children. The circles in the left-most column depict the intensity of overlap between V1 and V2v target networks in adults and children. Connectivity maps are overlaid on either an inflated brain surface or a high-resolution T1 template in MNI space, using a height threshold of p < 0.001 uncorrected and an extent threshold of *p* < 0.05 corrected. Notes: L, left; R, right.

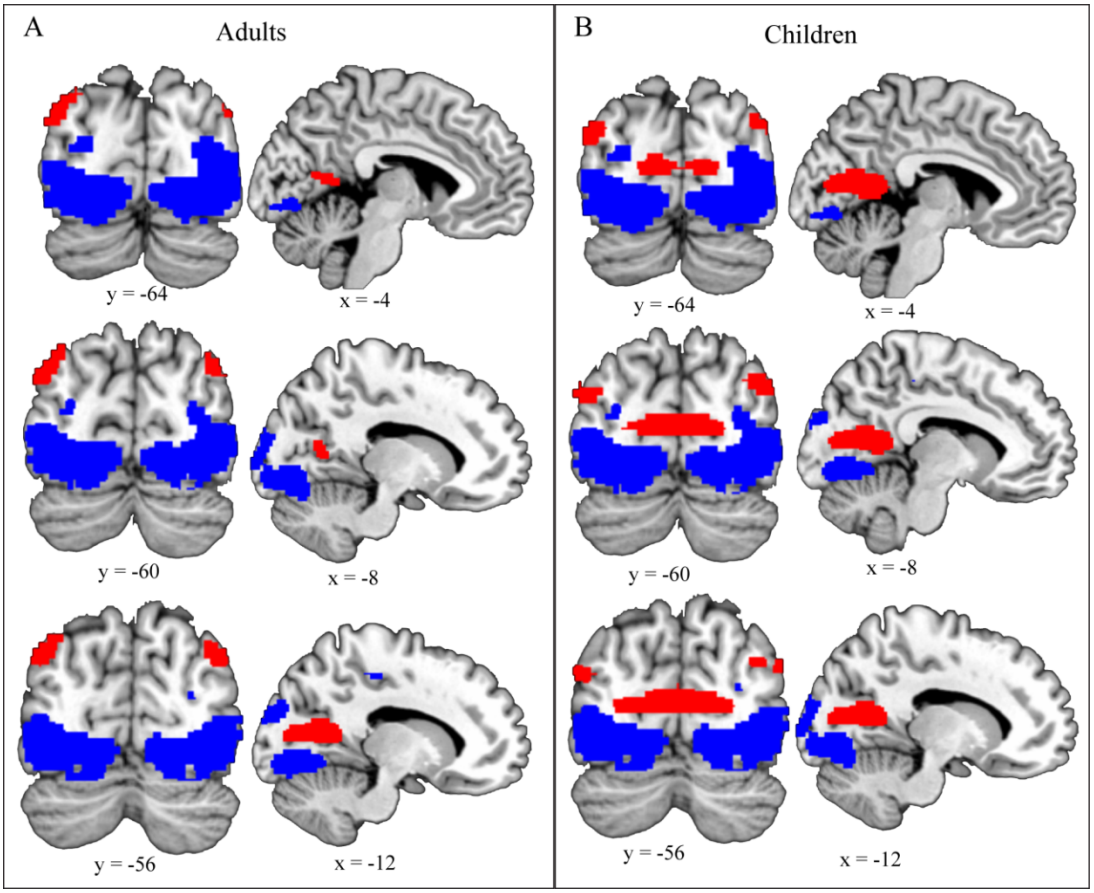

Fig S2. Differential patterns of functional connectivity between visual areas V1 and V2. Brain regions that showed stronger functional connectivity with V1, compared to V2, are shown in red, . Brain regions that showed stronger functional connectivity with V2, compared to V1, are shown in blue. Both adults (**A**) and children (**B**) showed very similar segregated connectivity profiles. No brain areas showed significant Group-by-Subregion interactions. Connectivity maps are overlaid on a high-resolution T1 template MNI space. Notes: L, left; R, right.

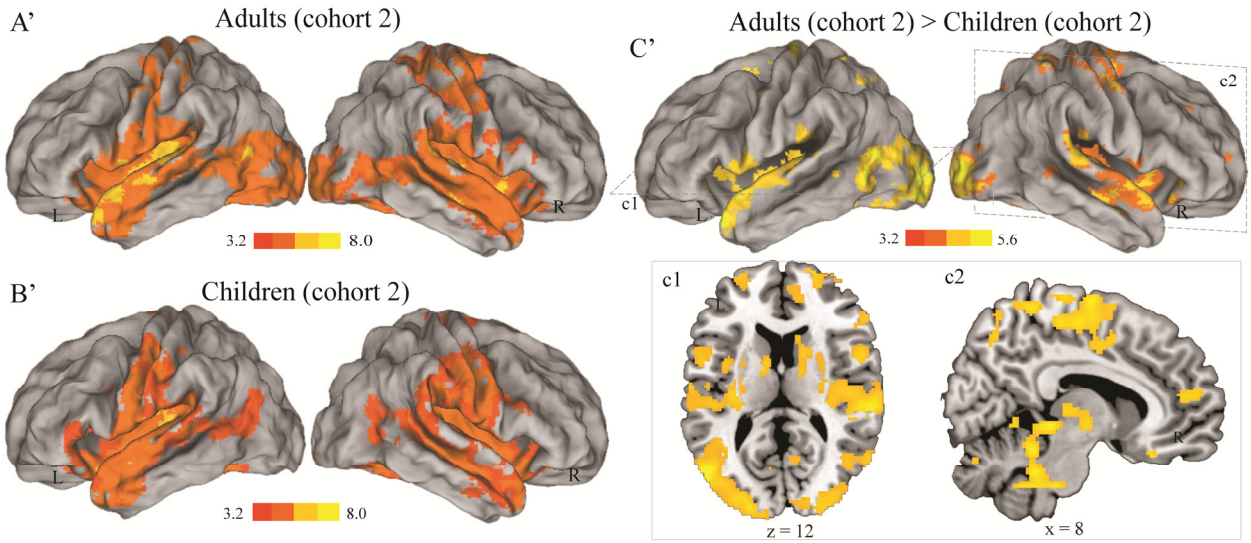

Fig S3. Immature functional connectivity of the amygdala in second cohort (i.e., cohort 2) children compared to adults. Brain regions showing significant intrinsic functional connectivity with the amygdala in adults (**A'**) and children (**B'**), and significant group differences in functional connectivity of the amygdala between adults and children (**C'**). Representative transversal and sagittal slices are depicted in (**c1**) and (**c2**). Intrinsic functional connectivity maps are overlaid on either an inflated brain surface or a high-resolution T1 template in MNI space. Notes: L, left; R, right.

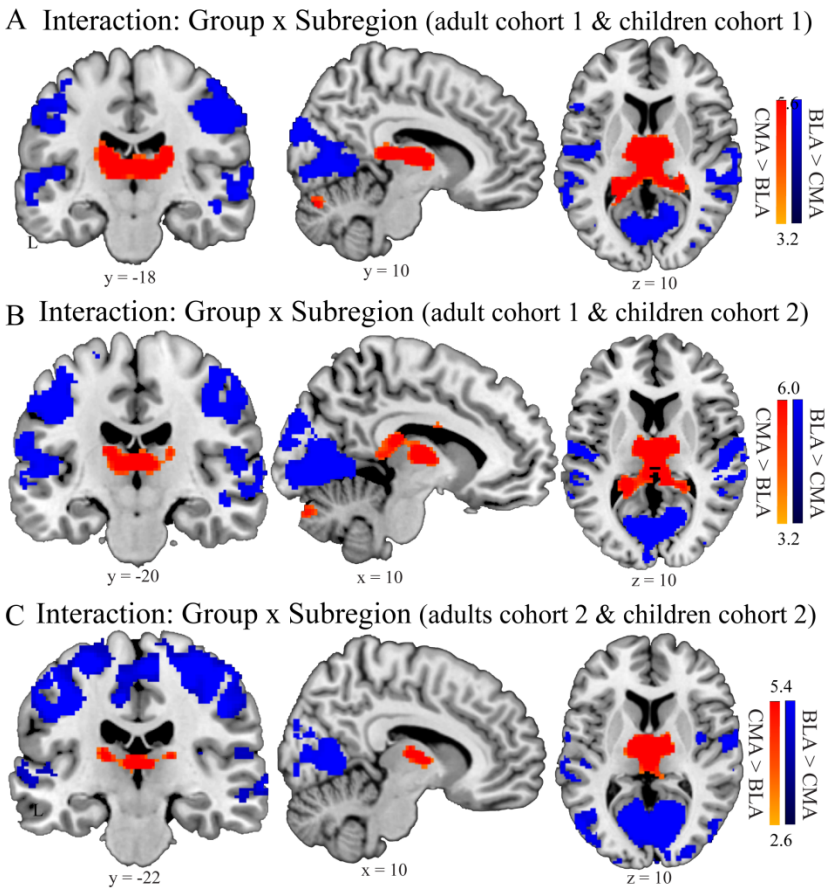

Fig S4. Immature differentiation between BLA and CMA functional connectivity networks in two cohorts of children compared to adults. Brain regions that showed significant group (adults, children) by subregion (BLA, CMA) interactions in (**A**) the first cohort (i.e., cohort 1) of adults and children, (**B**) the first cohort of adults and the second cohort (i.e., cohort 2) of children, and (**C**) in the second cohort of adults and the second cohort of children. Red represents the contrast of CMA with BLA. Blue represents the contrast of BLA with CMA. Intrinsic functional connectivity maps are overlaid on a high-resolution T1 template in MNI space. Notes: L, left; R, right.

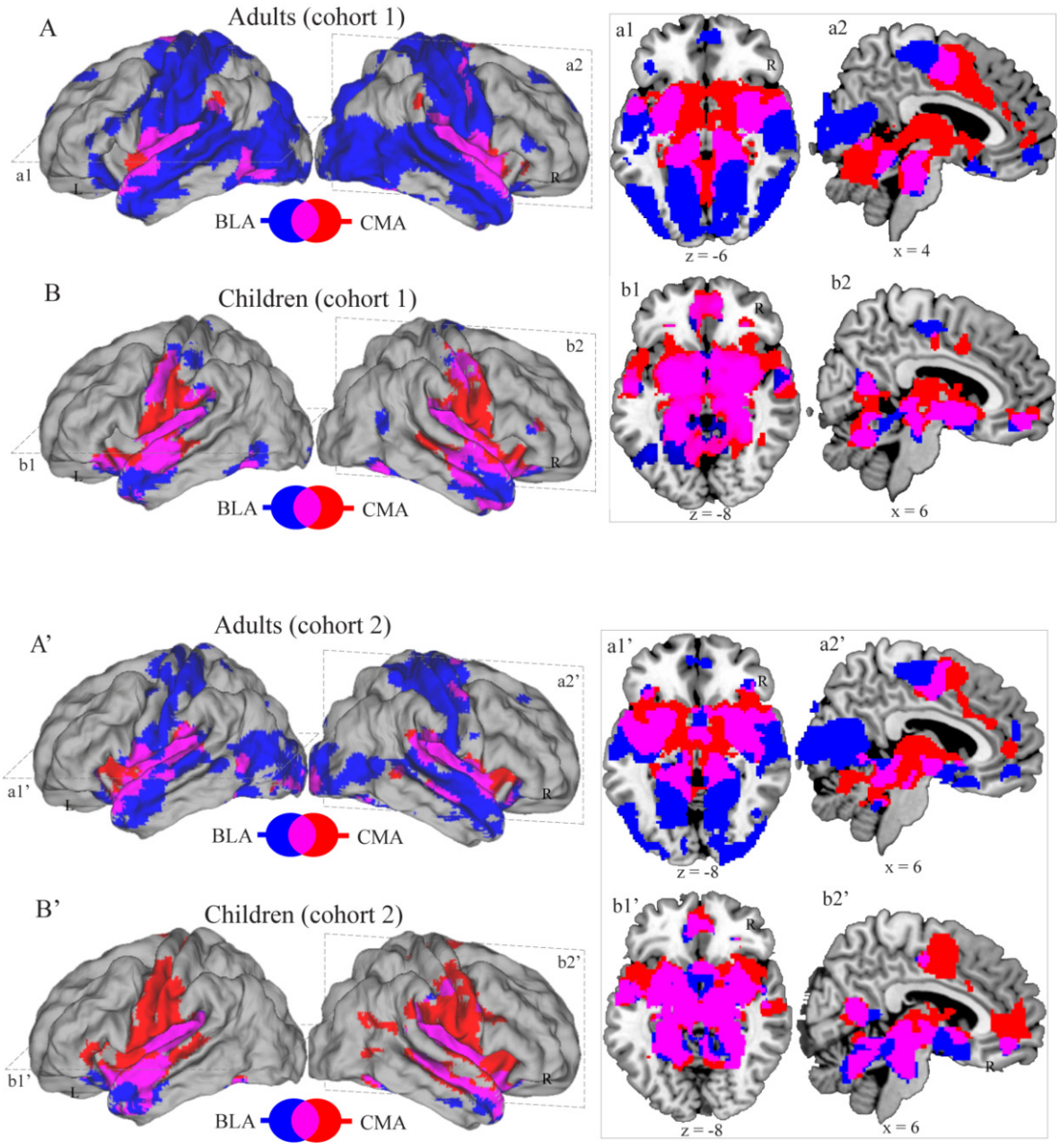

Fig S5. Similarity of amygdala subregional functional connectivity networks in second independent cohort of adults and children. Brain regions show significantly positive correlation with the CMA (shown in red) or the BLA (shown in blue; overlapping areas shown in pink) in the first cohort (cohort 1) of 24 adults (**A**), the first cohort of 24 children (**B**), the second cohort (cohort 2) of 16 adults (**A'**), the second cohort of 23 children (**B'**). Representative transversal and sagittal slices are depicted in (**a1**) and (**a2**) for adults, and in (**b1**) and (**b2**) for children. Connectivity maps are overlaid on either an inflated brain surface or a high-resolution T1 template in a stereotactic MNI space. Notes: L, left; R, right.

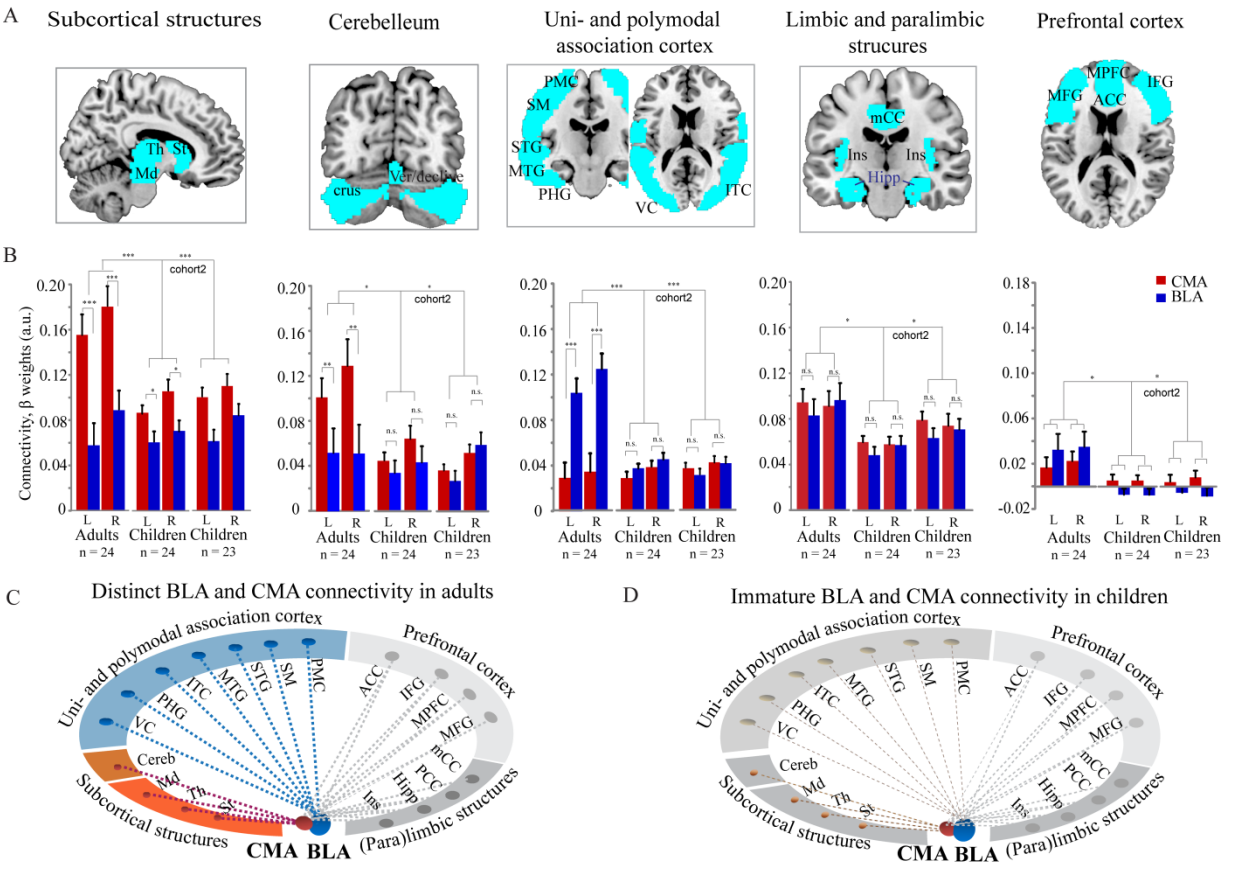

Fig *S6*. Differential patterns of BLA and CMA functional connectivity in adults and two cohorts of children. (**A**) Anatomically defined five target networks of interest - subcortical structures, cerebellum, unimodal and polymodal association areas, limbic and paralimbic structures and prefrontal cortices. (**B**) Averaged strength of functional connectivity between CMA (shown in red) or BLA (shown in blue) with target regions of interest. (**C**) & (**D**) Schematic illustration of weaker integration and differentiation of BLA and CMA connectivity in children compared to adults. ***(C)*** In adults, the BLA has stronger functional connectivity with polymodal association areas (shown in light blue with dotted lines connected), whereas the CMA showed stronger functional connectivity with subcortical structures (shown in orange with dotted lines connected). ***(D)*** In children, these differential patterns are significantly less pronounced (shown in lighter color with thinner lines). Abbreviations: **Limbic and paralimbic structures:** Ins = Insula, Hipp = Hippocampus, mCC = Middle cingulate cortex, PCC = Posterior cingulate cortex; **Uni- and polymodal association cortex:** VC, visual cortex, PHG = Parahippocampal gyrus, ITC = Inferior temporal cortex, MTG = Middle temporal gyrus, STG = Superior temporal gyrus, PMC = premotor cortex, SM = Sensorimotor cortex; **Subcortical structures:** St = Striatum, Th = Thalamus, Md = Midbrain; **Cerebellum:** Crus = Crus regions, Ver = Vermis/declive regions; **Prefrontal Cortex:** ACC = Anterior cingulate cortex, IFG = Inferior frontal gyrus, MPFC = medial prefrontal cortex, MFG = Middle frontal gyrus. Notes: * $p < 0.02$; ** $p < 0.01$; *** $p < 0.001$.

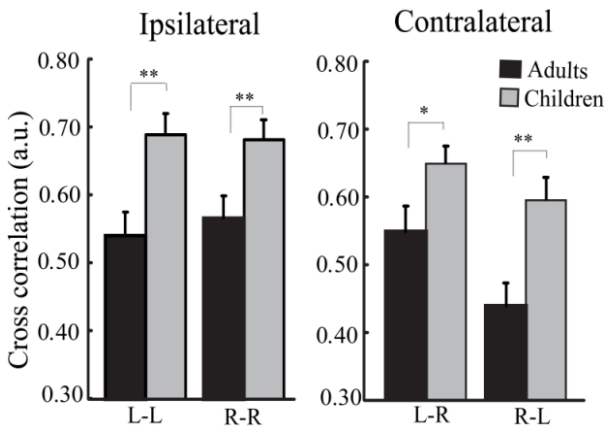

Fig S7. Stronger intra-amygdala intrinsic correlation in children compared to adults. Graphs represent averaged ipsilateral (left panel) and contralateral (right panel) correlation coefficients between CMA and BLA time series. Notes: L-L and R-R, ipsilateral correlation between CMA and BLA within left and right hemispheres respectively; L-R and R-L, contralateral correlations between CMA and BLA. * $p < 0.05$; ** $p < 0.01$.

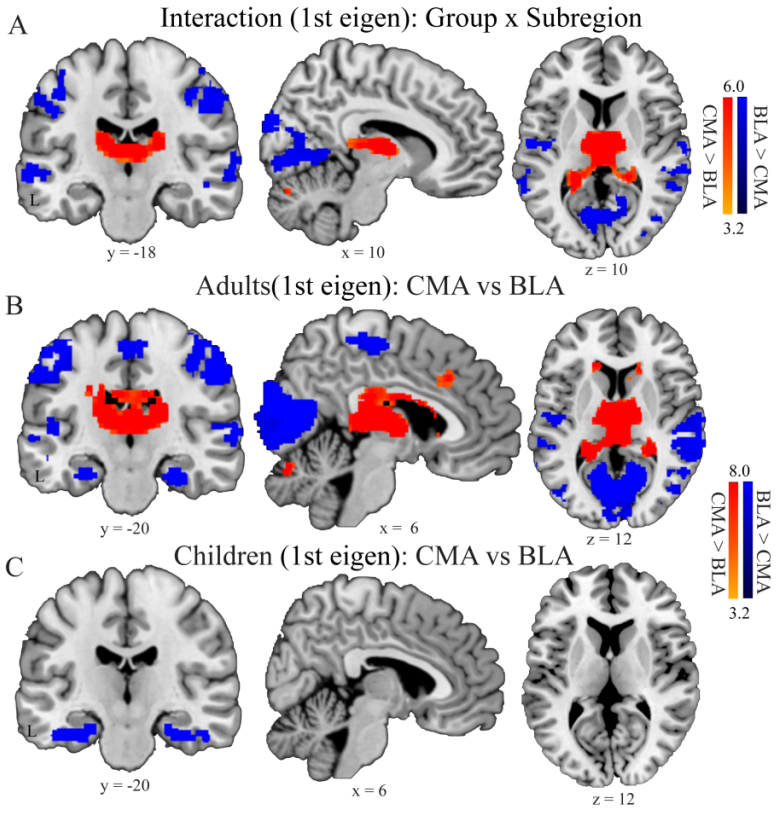

Fig S8. Results related to Group-by-subregion interactions based on analysis of the first eigenvalue (i.e., 1st eigen). Results from our new analysis based on of the first eigenvalue, rather than the mean of signals in each ROI, otherwise same as in ***Fig. 2*** in the manuscript.

References

1. Glover GH & Law CS (2001) Spiral-in/out BOLD fMRI for increased SNR and reduced susceptibility artifacts. *Magn Reson Med* 46(3):515-522.
2. Glover GH & Lai S (1998) Self-navigated spiral fMRI: interleaved versus single-shot. *Magn Reson Med* 39(3):361-368.
3. Amunts K*, et al.* (2005) Cytoarchitectonic mapping of the human amygdala, hippocampal region and entorhinal cortex: intersubject variability and probability maps. *Anat Embryol (Berl)* 210(5-6):343-352.
4. Kim JE*, et al.* (2010) Laterobasal amygdalar enlargement in 6- to 7-year-old children with autism spectrum disorder. *Archives of general psychiatry* 67(11):1187-1197.
5. Nichols T & Hayasaka S (2003) Controlling the familywise error rate in functional neuroimaging: a comparative review. *Stat Methods Med Res* 12(5):419-446.
6. Brett M, Anton JL, Valabregue R, & Poline JB (2002) Region of interest analysis using an SPM toolbox. *Neuroimage* 16:Abstract:497.
7. Maldjian JA, Laurienti PJ, Kraft RA, & Burdette JH (2003) An automated method for neuroanatomic and cytoarchitectonic atlas-based interrogation of fMRI data sets. *Neuroimage* 19(3):1233-1239.
8. LeDoux J (2007) The amygdala. *Curr Biol* 17(20):R868-874.
9. LeDoux JE (2000) Emotion circuits in the brain. *Annual review of neuroscience* 23:155-184.
10. Pessoa L & Adolphs R (2010) Emotion processing and the amygdala: from a 'low road' to 'many roads' of evaluating biological significance. *Nature reviews* 11(11):773-783.
11. Kriegeskorte N, Goebel R, & Bandettini P (2006) Information-based functional brain mapping. *Proc Natl Acad Sci U S A* 103(10):3863-3868.
12. Kriegeskorte N, Mur M, & Bandettini P (2008) Representational similarity analysis - connecting the branches of systems neuroscience. *Front Syst Neurosci* 2:4.
13. Xue G*, et al.* (2010) Greater neural pattern similarity across repetitions is associated with better memory. *Science (New York, N.Y* 330(6000):97-101.
14. Hale JR*, et al.* (2010) Comparison of functional connectivity in default mode and sensorimotor networks at 3 and 7T. *MAGMA* 23(5-6):339-349.
15. Burgund ED*, et al.* (2002) The feasibility of a common stereotactic space for children and adults in fMRI studies of development. *Neuroimage* 17(1):184-200.
16. Supekar K, Musen M, & Menon V (2009) Development of large-scale functional brain networks in children. *PLoS biology* 7(7):e1000157.
17. Dosenbach NU*, et al.* (2010) Prediction of individual brain maturity using fMRI. *Science (New York, N.Y* 329(5997):1358-1361.
18. Crone EA, Poldrack RA, & Durston S (2010) Challenges and methods in developmental neuroimaging. *Hum Brain Mapp* 31(6):835-837.
19. Ofen N*, et al.* (2007) Development of the declarative memory system in the human brain. *Nature neuroscience* 10(9):1198-1205.
20. Rottschy C*, et al.* (2007) Ventral visual cortex in humans: cytoarchitectonic mapping of two extrastriate areas. *Hum Brain Mapp* 28(10):1045-1059.